

AD-A105 248

NAVAL RESEARCH LAB WASHINGTON DC
ANALYSIS OF COAXIAL EMI FEEDTHROUGH FILTERS CONTAINING FERRITE --ETC(U)
OCT 81 G H STAUSS, J J KREBS, W G MAISCH

F/6 9/5

UNCLASSIFIED

NRL-MR-4651

NL

1-1
20
30 NDA

END

DATE

FILMED

0 81

DTIC

AD A105248

SECURITY CLASSIFICATION OF THIS PAGE (When Data Entered)

14

NRL-MR-4651

REPORT DOCUMENTATION PAGE		READ INSTRUCTIONS BEFORE COMPLETING FORM
1. REPORT NUMBER NRL Memorandum Report 4651	2. GOVT ACCESSION NO. AD A105248	3. RECIPIENT'S CATALOG NUMBER
4. TITLE (and Subtitle) ANALYSIS OF COAXIAL EMI FEEDTHROUGH FILTERS CONTAINING FERRITE ELEMENTS.	5. TYPE OF REPORT & PERIOD COVERED Interim report on a continuing NRL problem.	
7. AUTHOR(s) G. H. Stauss, J. J. Krebs, and W. G. Maisch	8. CONTRACT OR GRANT NUMBER(s)	
9. PERFORMING ORGANIZATION NAME AND ADDRESS Naval Research Laboratory Washington, DC 20375	10. PROGRAM ELEMENT, PROJECT, TASK AREA & WORK UNIT NUMBERS 62543N; XF43 453 401 68-0563-A-1	
11. CONTROLLING OFFICE NAME AND ADDRESS	12. REPORT DATE October 10, 1981	13. NUMBER OF PAGES 32
14. MONITORING AGENCY NAME & ADDRESS (if different from Controlling Office)	15. SECURITY CLASS. (of this report) UNCLASSIFIED	
	15a. DECLASSIFICATION/DOWNGRADING SCHEDULE	
16. DISTRIBUTION STATEMENT (of this Report) Approved for public release; distribution unlimited.		
17. DISTRIBUTION STATEMENT (of the abstract entered in Block 20, if different from Report)		
18. SUPPLEMENTARY NOTES		
19. KEY WORDS (Continue on reverse side if necessary and identify by block number) EMI (Electromagnetic Interference) Feedthrough filters Ferrite elements		
20. ABSTRACT (Continue on reverse side if necessary and identify by block number) An analysis of coaxial EMI feedthrough filters containing high permeability ferrite and high permittivity dielectric elements is given. The frequency dependent complex permeability and permittivity of useful materials are modeled, and the effect of these parameters as well as load and source impedance, filter dimensions and number of filter elements on the insertion loss behavior are investigated. Filter problems are treated as are suggestions for improved performance.		

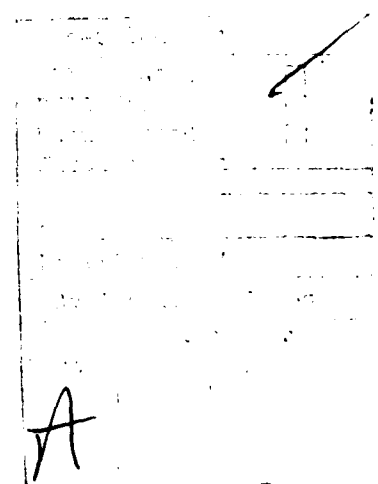
DD FORM 1 JAN 73 1473

EDITION OF 1 NOV 69 IS OBSOLETE
S/N 0102-014-6601

25-195C
SECURITY CLASSIFICATION OF THIS PAGE (When Data Entered)

CONTENTS

I. INTRODUCTION AND SUMMARY	1
II. FEEDTHROUGH FILTERS	4
III. PROPERTIES OF HIGH PERMEABILITY AND HIGH PERMITTIVITY MATERIALS	8
IV. FILTER CALCULATIONS AND DISCUSSION	10
V. CONCLUSIONS AND SUGGESTIONS FOR FEEDTHROUGH FILTER IMPROVEMENTS	16



ANALYSIS OF COAXIAL EMI FEEDTHROUGH
FILTERS CONTAINING FERRITE ELEMENTS

I. INTRODUCTION AND SUMMARY

In typical shipboard situations there are substantial possibilities for electromagnetic interference (EMI) between powerful rf sources and signal processing equipment, including computers. This interference normally occurs via audio frequency rectification in which a high intensity external rf field reaches the victim circuit through the signal or power leads. The rf is then rectified by the first non-linear element (usually a diode or transistor) in that circuit and the rf envelope appears as a false signal. The standard solution for such EMI problems is to install feedthrough filters on the signal/power leads. Since these filters must pass the signal frequencies without substantial loss while strongly attenuating the rf signals, they are low pass filters. Except for the feedthrough filters the victim circuit is contained in a closed rf shielding box so that the capabilities of the filter are the determining factor in controlling EMI.

The purpose of the present study is to perform a thorough analysis aimed at achieving improved performance or lower cost or both for feedthrough filter connectors containing ferrite elements. Improved performance includes increased rf attenuation and/or a more rapid rise in attenuation with increasing frequency beyond the passband of the filter. The baseline standard for improvement is the performance of already existing filter pin connectors, since such filters are particularly amenable for use in retrofit applications when many leads are introduced into the shielding box via a single multipin connector.

The bulk of this report represents an analysis of the filter behavior of such filter pin connectors taking into account the fact that both the permeability μ of the ferrite components and the permittivity ϵ of the dielectric components are frequency dependent quantities which also are complex, i.e.,

Manuscript submitted September 14, 1981.

which have both real and imaginary parts.* We proceed in several steps in order to clarify the role both of these quantities and of the filter dimensions on performance. First, (Chapter II) the low frequency performance, which can be described in terms of frequency dependent lumped circuit parameters, is mathematically modelled. It is then shown that, because of the reduced transmission velocity of electromagnetic waves in materials having large permeabilities or permittivities, the components used in these filters exhibit dimensional resonances in the UHF band for typical lengths. As a result, a general transmission line model is used which makes the effects of dimensional resonances explicit and allows for complex, frequency dependent $\tilde{\mu}$ and $\tilde{\epsilon}$ parameters. This approach is valid throughout the frequency range studied (0.1-10,000 MHz).

Next (Chapter III), values of $\tilde{\mu}$ and $\tilde{\epsilon}$ for practical materials are given, including their dependences on frequency. These data are then mathematically modelled. They are then (Chapter IV) combined with the lumped circuit and transmission line models to calculate insertion loss vs. frequency for a number of illustrative filter pin connector configurations. These are selected to stress the roles of $\tilde{\mu}$, $\tilde{\epsilon}$, the circuit dimensions, impedance matching (effect of source and load impedances) and multiple filter sections on filter performance. Finally (Chapter V), we give our conclusions, and methods for improving existing filters are suggested.

The conclusions are summarized briefly below:

1. Large impedance mismatches between adjacent filter elements and between these and the rf source and load are essential to achieving large insertion loss in the EMI filter stopband. In feedthrough filter pins high permittivity dielectric materials and high permeability ferrite magnetic materials are used to achieve this.

2. The mature nature of the development of materials in both these fields makes it unlikely that there will be material improvements which will have a significant impact on filter performance.

3. Leads which carry currents greater than an ampere or so can cause magnetic saturation of the ferrite and greatly decrease filter insertion loss in the stopband. Such power leads require special attention since a single

*Throughout this report $\tilde{\mu}$ and $\tilde{\epsilon}$ are the relative permeability and permittivity, respectively. When one wishes to use the actual permeability and permittivity the relative values must be multiplied by the corresponding free space values μ_0 and ϵ_0 .

poorly filtered lead can destroy the effectiveness of all the other EMI efforts to protect a circuit. (H. M. Schlicke has suggested a possible solution to this problem. See Chapter V.)

4. It is essential to evaluate the effect of source and load impedance on filter performance and not rely on specification based only on 50 ohm terminations.

5. Multi-element filters (more than 3 elements) can be used to improve the sharpness of insertion loss cut-on and the insensitivity to variations in the load and source impedances.

6. The properties of filter pin connectors are essentially determined by their behavior near the stopband edge for which the elements are in the low frequency regime.

7. In general, EMI filters will distort wideband signals due to variations in the phase shift with frequency.

8. The coaxial filter design used for analysis in this report, predicts comparable or better insertion loss and a sharper insertion loss turn-on than commercial filter pins. Furthermore, the simplicity of the design suggests that multi-element filters could be made at lower cost. As a result, it is recommended that the calculations be tested by constructing and testing such filters.

The authors have profited greatly from a careful perusal of the out-of-print book "Essentials of Dielectromagnetic Engineering," by H. M. Schlicke (Wiley, New York, 1961) and the analysis used here reflects many of the ideas used in that book.

II. FEEDTHROUGH FILTERS

A. Low Frequency (Lumped Element) Circuit Models

The simplest possible feedthrough filter is shown in Fig. 1. It consists of a feedthrough capacitor which shunts the load impedance R_L . The rf source has a voltage V_1 and source impedance R_s . Although R_s and R_L are written as if they are resistances and are taken to be real in our later calculations, they can in general be complex quantities.

The output (load) rf voltage V_2 which appears in the victim circuit is easily calculated for Fig. 1.

$$V_1/V_2 = 1 + R_s (G_L + G_C) \quad (1)$$

where $G_L = 1/R_L$ and $G_C = j\omega C$. In the absence of the filter capacitor ($C = 0$)

$$(V_1/V_2)_0 = 1 + R_s G_L = (R_s + R_L)/R_L \quad (2)$$

The rf attenuation (insertion loss) A_f of the filter is defined in general as the ratio of

$|V_1/V_2|^2$ with the filter, to $|V_1/V_2|_0^2$ without the filter, expressed in decibels, i.e.,

$$A_f(\text{db}) = 20 \log |V_1/V_2| / |V_1/V_2|_0 \quad (3)$$

This definition is in accord with MIL STD 220, which also specifies $R_L = R_s = 50$ ohms. Although we usually take $R_L = 50$ ohms, the effect of varying R_s and R_L is significant and is investigated later.

If for simplicity we take $R_L = R_s$, then Fig. 1 yields

$$A_f(\text{db}) = 20 \log \left| \frac{1}{2}(2 + j\omega C R_s) \right| \quad (4)$$

so that the filter attenuation increases $\sim 20\text{dB/decade}$ for $\omega C R_s > 4$. Such a small slope for the filter insertion loss cutoff may well be inadequate for intense rf sources whose operating frequency is within the decade above the victim circuit operating frequency. One can retain the low feedthrough impedance of the filter at low frequencies while improving the high frequency attenuation by introducing a ferrite inductor element into the filter as shown in Fig. 2.

A ferrite material is characterized by a complex permeability $\tilde{\mu} = \mu' - j\mu''$ where μ' and μ'' have frequency dependence typically as shown in Fig. 3. The impedance of such an element is

$$Z_f = j\omega\mu_0\tilde{\mu}L_0 = j\omega\mu_0L_0(\mu' - j\mu'') \equiv j\omega L + R$$

so that L and R are both functions of ω (see Fig. 2). Here we have assumed a ferrite bead (coaxial ferrite tube) slipped on a bare wire and the value of L_0 is comparable to the self-inductance of the wire alone. Because of the behavior shown in Fig. 3, the ferrite looks like an inductor at low frequencies and like a resistor for frequencies much above f_c . Thus, if the circuit operating frequency is low enough that $\omega L \ll R_c$ the signal will not be influenced by the ferrite. The key aspect of the ferrite element is that it allows one to add additional sections to the filter and thus increase the attenuation/decade beyond the passband. Multiple filter sections will be discussed in part C of this chapter.

B. General (Transmission Line) Circuit Models

The lumped element circuit analysis which produces Eq. (4) for the attenuation of the filter circuit of Fig. 1 leads one to expect an ever-rising attenuation for $\omega > 4 (R_s C)^{-1}$. Unfortunately, nature is not so kind. In order to achieve sufficiently large shunt capacitance (>200 pF) with a typical filter length of 1 cm, a high permittivity ceramic based on barium titanate must be used. If one uses $\epsilon' = 1700$ as a reasonable value, a 1 cm length is a half wavelength long at 350 MHz. The resulting dimensional resonance at this frequency causes the low frequency shunt capacitor to "disappear" so there is sharp loss in attenuation. Similar resonances occur at higher frequencies which are harmonics of this lowest resonance. These lead to a series of "punch-through" frequencies where the filter passes rf. Fortunately, the losses exhibited by high ϵ dielectrics aid in designing around this difficulty.

A transmission line approach allows these dimensional resonances to be taken into account explicitly and is essential to any analysis which extends into the UHF and microwave bands. A coaxial transmission line is chosen here for ease of analysis and because it is well-suited for feedthrough filter pin applications. Figure 4 defines the needed dimensions of such a coaxial line. The space between the inner and outer conductors is filled with a material having (in general) complex $\tilde{\epsilon}$ and $\tilde{\mu}$.

The behavior of such a transmission line is determined by its characteristic impedance Z_c and propagation coefficient γ . These are given by

$$Z_c = \frac{1}{2\pi} (\tilde{\mu}/\tilde{\epsilon})^{\frac{1}{2}} (\mu_0/\epsilon_0)^{\frac{1}{2}} \ln(r_2/r_1) \quad (5)$$

and

$$\gamma = j(\tilde{\mu}\tilde{\epsilon})^{\frac{1}{2}} (\mu_0\epsilon_0)^{\frac{1}{2}} \omega \quad (6)$$

One can consider the filter to consist of a string of such sections filled alternately with high $\tilde{\epsilon}$ and high $\tilde{\mu}$ materials. This transmission line approach is valid at low as well as high frequencies.

C. Multiple Section Filter Analysis

As additional sections are added to a filter the analytical expressions for the filter attenuation rapidly become very complicated and uninformative. If numerical methods are to be used to evaluate the frequency dependence of the attenuation, it is best to choose a computational technique which makes it simple to add on extra filter elements in a straightforward way. This can be done by means of four-terminal (four-pole) matrix methods. For example, suppose we have the four-pole network shown in Fig. 5. It can be completely characterized by a matrix A defined as follows:

$$A = \begin{bmatrix} a_{11} & a_{12} \\ a_{21} & a_{22} \end{bmatrix} = \begin{bmatrix} (V_1/V_2)_{I_2=0} & (V_1/I_2)_{V_2=0} \\ (I_1/V_2)_{I_2=0} & (I_1/I_2)_{V_2=0} \end{bmatrix} \quad (7)$$

If one has two such four-poles cascaded as in Fig. 6, then the A matrix for the total circuit is given by matrix multiplication of A_1 and A_2 , i.e., $A = A_2 \times A_1$. Thus, extra four-pole sections are easily added.

This form is particularly useful for the filter problem since if we construct an A matrix for the entire filter including the load and source impedances, then its a_{11} element is related to the insertion loss by the expression

$$A_f(\text{db}) = 20 \log a_{11} R_\ell / (R_s + R_\ell) \quad (8)$$

Lumped Elements - It is very easy to show based on Eq. (7) that the lumped element four-pole in Fig. 7 has the A matrix

$$A = \begin{bmatrix} 1 + Z_1 G_2 & Z_1 \\ G_2 & 1 \end{bmatrix} \quad (9)$$

where $G_2 = 1/Z_2$. Any cascaded lumped element filter can be built up of sections of the type shown in Fig. 7 with suitably chosen Z_i 's. For example, the A matrix for Fig. 1 is given by

$$A = \begin{bmatrix} 1 & R_s \\ 0 & 1 \end{bmatrix} \times \begin{bmatrix} 1 & 0 \\ j\omega C & 1 \end{bmatrix} \times \begin{bmatrix} 1 & 0 \\ G_\ell & 1 \end{bmatrix}$$

so that $a_{11} = 1 + R_s (G_\ell + j\omega C)$ and when this is used with Eq. (8) and $R_\ell = R_s$ one gets Eq. (4) for this simple case. In our computer calculations, where

all the matrix elements are represented by numbers, an extension to an arbitrary number of sections is trivial.

Transmission Lines - The A matrix for a transmission line of length ℓ is

$$A = \begin{bmatrix} \cosh \gamma \ell & Z_c \sinh \gamma \ell \\ (Z_c)^{-1} \sinh \gamma \ell & \cosh \gamma \ell \end{bmatrix} \quad (10)$$

where Z_c and γ are given by Eqs. (5) and (6). Note that in the low frequency limit where $\gamma \ell \ll 1$, then Eq. (10) becomes

$$A = \begin{bmatrix} 1 & Z_L \\ G_C & 1 \end{bmatrix}$$

where $Z_L = j\omega [(\ell/2\pi) (\tilde{\mu}\mu_0) \ln(r_2/r_1)] \equiv j\omega L$ and $G_C = j\omega [2\pi\ell(\tilde{\epsilon}\epsilon_0)/\ln(r_2/r_1)] \equiv j\omega C$. Note that L and C are just the inductance and capacitance of the coaxial transmission line as one might expect.

In the next chapter we consider actual values of $\tilde{\mu}$ and $\tilde{\epsilon}$ for real materials.

III. PROPERTIES OF HIGH PERMEABILITY AND HIGH PERMITTIVITY MATERIALS

We now consider the properties of actual materials having high permeability or high permittivity which are needed for constructing filter pin feedthrough filters.

A. High Permeability Materials

The production of ceramic magnetic materials which have high initial permeabilities $\tilde{\mu}$ is a well-developed commercial enterprise. The frequency dependence of the real (μ') and imaginary (μ'') parts of $\tilde{\mu}$ ($=\mu'-j\mu''$) are shown in Figs. (8) and (9) for several of the best commercial and laboratory materials of this type (cf Fig. 3). The classes of materials with the highest initial permeabilities are the Mn-Zn and Ni-Zn spinel ferrites of the types $(\text{Mn, Zn, Fe})_3\text{O}_4$ and $(\text{Ni, Zn, Fe})_3\text{O}_4$. For frequencies above 500 MHz the hexagonal cobalt Z-type ferrites (U60) have superior μ' and μ'' values.

It should be noted that in general the maximum available μ' (and μ'') fall off as one goes to higher frequencies. Indeed, for frequencies above 1 GHz there are no existing ceramic materials with μ' or μ'' greater than 14. (This ignores a field-aligned version of U60.) This compilation represents a selection from a rather extensive literature search and we expect that the permeabilities given are close to the technological limit on these material classes. This is consistent with the fact that this is a rather mature materials development field.

In order to simplify later numerical analysis it is useful to represent the frequency dependent values of μ' and μ'' by approximate analytical forms for several of the materials shown in Figs. 8 and 9. Reasonable approximations are given by the formulas

$$\mu' = \mu'_I / [1+(f/f_c)^2] + 1 \quad (11a)$$

$$\mu'' = \mu''_I (f/f_c) / [1+(f/f_c)^2] \quad (11b)$$

where the μ'_I , μ''_I and f_c values which characterize various materials are given in Table I.

The dielectric constant ϵ of each ferrite material is assumed to be real and taken to be 10, independent of frequency. This is reasonable for the Ni-Zn and Z-type ferrites ($10 \leq \epsilon' \leq 20$). However, many high $\tilde{\mu}$ Mn-Zn ferrites (such as N22 and T38) exhibit very large and complex frequency-dependent effective dielectric constants due to a combination of low intrinsic resistivity ($\rho \sim 10^{-3}$ ohm-cm) with the existence of thin high resistance layers which

separate the grains in the ceramic. This results in effective dielectric constants which may reach 10^5 at low frequencies and which roll off rather slowly above roughly 1 MHz. Such values would lead to undesirable geometric resonances in the ferrite portion of the filter in the 1-10 MHz range, but the associated low resistivity damps these heavily. Such low resistivity results in attenuation throughout the filter passband and complicates efforts to achieve low frequency stopbands.

Table I. Permeability Parameters for Selected Ferrites

Ferrite	μ'_I	μ''_I	f_c (MHz)	$\tilde{\epsilon}'$
T38	10000	18000	0.2	a
N22	1400.	1400.	4.	a
B2	240.	240.	50.	10.
K1	80.	80.	100.	10.
U60	10.	20.	1500.	10.

a. See Sec. IIIA.

B. High Permittivity Materials

Most high permittivity ceramic materials represent some variant based on the pure ferroelectric material barium titanate (BaTiO_3). Materials with real permittivities ϵ' in the range 1000-6000 are easily available although for $\epsilon' > 2000$ they begin to show considerable temperature dependence. These materials show frequency dependences in $\tilde{\epsilon}$ similar to Fig. 3, but do not show dispersion (i.e., roll-off) until the gigahertz region where ϵ'' has its maximum. The frequency dependence of $Q_e \equiv \epsilon'/\epsilon''$ for a typical ceramic material is shown in Fig. 10.

We again use analytical expressions to approximate the behavior of barium titanate. They are

$$\epsilon' = (2/3) \epsilon'_I / [1+(f/f_c)^2] + \epsilon'_I/3 \quad (12a)$$

$$\epsilon'' = (2/3) \epsilon'_I (f/f_c) / [1+(f/f_c)^2] + \epsilon'_I/50 \quad (12b)$$

In this report the representative values $\epsilon'_I = 1700$ and $f_c = 3$ GHz are used. For these materials one can take $\tilde{\mu} = 1$.

IV. FILTER CALCULATIONS AND DISCUSSION

In this chapter the frequency dependence of the filter insertion loss for a variety of feedthrough filter pin conditions is calculated. In order to clarify the principles which govern the behavior of these filters, the important parameters are varied one by one and the changes they induce are compared with a reference case calculation. The implications of these variations for practical EMI situations are also discussed.

In order to allow the parameters to be varied in a straightforward manner, a simple multi-element coaxial transmission line filter design was chosen and the overall circuit is illustrated in Fig. 11. To correspond to realistic dimensions for a filter pin, the length of the actual filter is fixed at 1.5 cm while the outer diameter of the pin is fixed at 0.3 cm. These dimensions are compatible with commercial design dimensions. The computer program used allows up to five coaxial elements and can readily be extended to an arbitrary number. The odd numbered elements are capacitors at low frequencies. The dielectric used to fill those coaxial sections has the frequency dependence given by Eqs. (12a,b) with $\epsilon'_0 = 1700$ and $f_c = 3000$ MHz. The section lengths and OD to ID ratios r_2/r_1 are given in the figure captions where the source and load resistors used are also listed. The even numbered elements are inductors at low frequencies. The ferrites used in them and their dimensions are shown in the captions while their material parameters are specified in Table I. The frequency dependence of μ' and μ'' are given by Eqs. (11a,b).

The computer program makes use of the transmission line formulas and four-pole analysis spelled out in Chapter II. Note that by setting the length of any element equal to zero, its A matrix becomes a unit matrix (see Eq. (10)). This essentially eliminates that element from the problem. Thus by using $\ell_1 = 0$ but $\ell_2 \neq 0$ the program can treat a filter with an inductor adjacent to the load.

Under the condition that a piece of coaxial transmission line is propagating signals in its principal mode and is terminated in a load Z_ℓ much smaller than its characteristic impedance Z_c , at low frequencies it will look like an inductor with inductance $L = (\ell \tilde{\mu} \mu_0 / 2\pi) \ln(r_2/r_1)$ in series with the load. On the other hand, a line having $Z_\ell \gg Z_c$ will appear at low frequencies like a shunt capacitor with $C = 2\pi \ell \tilde{\epsilon} \epsilon_0 / \ln(r_2/r_1)$. For typical materials and for the lengths quoted, the low frequency approximation will persist to about 10-100 MHz, while, for terminating loads between ~10 and 200 ohms, successive

elements in the coaxial series see loading conditions such that the above low frequency limits are realized. Thus a three-segment coaxial series transforms smoothly into a low frequency C-L-C pi filter.

This low frequency correspondence to a pi filter is significant since the critical characteristics of the filter performance, viz. the frequency for the onset of attenuation, the low frequency dispersion, and the rate of attenuation change with frequency at the beginning of the stopband are usually determined in the low frequency regime. It is important to emphasize that this performance results from mismatches between the coaxial segments and between them and the terminations, so that if these fail the attenuation is destroyed.

Reference case - The reference model (Fig. 12) chosen to illustrate the behavior of filter pin feedthrough connectors, is such a three segment (pi type) series of coaxial elements. The lengths of the segments are all chosen equal (0.5 cm to satisfy the constraint on total length). A ferrite with intermediate response (type B2, $\mu'_0 = \mu''_0 = 240$, $f_c = 50$ MHz, $\epsilon' = 10$) was chosen. With the dimensions and materials chosen $C = 2600$ pF and $L = 0.43$ μ H at low frequencies. Both the load and source impedances are taken to be 50 ohms. No allowance for ferrite magnetic saturation is made here, although this can be an important consideration, and the ferrite is assumed always to act as an isotropic medium.

In order to make intercomparisons of the various filters as simple as possible a standard format has been adopted for presenting the frequency dependence of the insertion loss A_f . This format covers the frequency range from 0.1 to 10,000 MHz on a logarithmic scale and covers filter insertion losses up to 120 dB. This is shown in Fig. 12 for the reference case.

There are several features to note in Fig. 12. The dip near 7 MHz followed by a rapid rise in insertion loss of approximately 60 dB/decade is due to the series resonance of the L and C's (i.e., $\omega L \approx 2/\omega C$). This low frequency behavior depends on the circuit loading. If the two end capacitors are equal and $R_l = R_s = R$, then extrema in A_f with frequency will occur only if $R^2 > L/2C$. For other loading conditions it is possible to produce a single extremum with $A_f < 0$, i.e. apparent amplification (!) by the filter, see Fig. 20 below. In the particularly simple but not untypical case when $R^2 = L/2C$ then $A_f = 10 \log (1 + \omega^6 L^3 C^3 / 8)$ and hence will stay close to 0 dB up to $\omega^2 LC \approx 2$ and then rise 60 dB/decade for $\omega^2 LC > 4$.

The next pronounced feature in Fig. 12 is the dip at 730 MHz which corresponds to a $\lambda/2$ geometric propagation resonance in either of the two dielectric segments. (The ferrite dip is at ~ 15 GHz). The effect of this strong dip can be lessened easily by making the dielectric segments of unequal lengths. This is illustrated in Fig. 13 where all the parameters are kept constant except $l_1=0.4$ cm and $l_3 = 0.6$ cm. In later figures, similar strong dips could be reduced in the same way. Shortening all segments by a common factor results in a uniform shift of all features to higher frequencies.

The sharp rise in filter insertion loss for $f > 1$ GHz is due to propagation losses in the dielectric material (see below).

The low frequency behavior of the reference case can be described well by a lumped element model. Thus Fig. 14 shows the insertion loss for a pi lumped element filter with $C=2600$ pF and $L=0.43$ μ H (same values as for the reference case). Below 50 MHz Figs. 14 and 12 are in good agreement. At higher frequencies propagation effects become important. The lumped element model ignores these effects and hence gives unrealistically high insertion loss values above 100 MHz.

Effect of ferrite and dielectric losses - The ferrite and high ϵ dielectric materials used in the reference case introduce a typical amount of rf attenuation via the lossy imaginary part of the propagation constant. Those losses, however, are responsible for only a small part of the calculated attenuation in Fig. 12. This is shown in Fig. 15 where the same material parameters are used as in the reference case but the r_2/r_1 ratios for the three segments are changed and R_s and R_l are reduced so that all segments are matched to the load. One sees that only for frequencies above 1000 MHz do propagation losses make a significant impact on the total filter insertion loss. At all frequencies below 3 GHz the geometric structure of the filter, which determines the low frequency L and C, is crucial. That is, one must have substantial mismatches between adjacent segments; when they are absent the filter action is destroyed as Fig. 15 indicates.

Despite the observation above, it is not true that material losses are negligible. A mismatched but lossless line will possess a whole series of periodic, sharp (punch-through) pass bands in which the filter insertion loss decreases to zero; it is the dispersion and attenuation of the ferrite and of the dielectric which have reduced these very sharp features to irregularities in Fig. 12. The reference case, recalculated in Fig. 16 with the dielectric

losses eliminated, illustrates the importance of these losses. Removal of the ferrite losses instead, as in Fig. 17, mainly increases the attenuation in the region ~300 MHz where the real ferrite dispersion is pronounced. There are fewer pass bands here but a general sharpening of these is also evident.

Effect of other ferrites - The existence of a number of different ferrites with a variety of μ'_0 , μ''_0 and f_c values makes it possible to alter the filter characteristics without changing any of the filter dimensions. As examples of this, Fig. 18 shows the reference case with the ferrite K1 substituted for B2 while Fig. 19 is again the same except for the use of μ values belonging to the ferrite N12. Note that use of these latter values shifts the onset of attenuation to lower frequencies and eliminates the low frequency dip in the filter insertion loss. This is largely due to the rapid change in μ' and the significant value of μ'' for this ferrite in the 1-10 MHz region. However, as noted in Sec.IIIA., proper $\tilde{\epsilon}$ values for N22 greatly increase the attenuation throughout Fig. 19, to the extent that 120 dB is reached at 100 MHz. This loss can be reduced by insulating the ferrite; this creates a compound element, not amenable to simple analysis, in which ϵ' is no longer very large.

Insertion loss above 1 GHz - As can be seen in all the figures presented above, insertion loss above 1 GHz is very substantial and increases rapidly with frequency. Thus frequencies up to 10 or 20 GHz should be well attenuated by any filter effective at 1 GHz. Above a few GHz, new transmission line modes not treated above, especially TE_{n1} modes, will begin to reach their cutoff frequencies; their attenuation near cutoff will be high and at higher frequencies will approximate that of the TEM mode, so any such modes should not seriously degrade the filter action. One can also anticipate that such higher order modes will be more difficult to excite in a coaxial structure than will the TEM mode.

Effects of Load and Source Impedance - The effect of reducing the load impedance from 50 ohms to 5 ohms is shown in Fig. 20 for a filter which is otherwise like the reference case. The result is a significant loss in insertion loss at most frequencies as well as a change in the low frequency behavior. The first effect arises from reducing the impedance mismatch between the last transmission line segment and the load. The second effect illustrates a case in which there is actual resonant enhancement rather than attenuation for rf frequencies between 1 and 7 MHz. For a symmetric filter such as we have

here interchanging the source and load impedance leaves the A_f unchanged, so that reducing R_s to 5 ohms while keeping R_l at 50 ohms will give the same results.

While it is reasonable to take R_s and R_l in the 50-300 ohm range for signal circuits, in the case of power leads one may have R_s and R_l values as low as 0.1 ohm. Since the characteristic impedances of the dielectric segments of transmission line are typically a few tenths of an ohm (0.27 ohm in the reference case), the filter insertion loss is greatly reduced due to the lack of mismatch. This is illustrated in Fig. 21 which is like the reference case but with $R_l = R_s = 0.1$ ohm. This is clearly a far less effective filter. However, by using an L-C-L tee filter with the same L and C segment dimensions and materials as in the reference case one obtains Fig. 22 with a much improved stopband. In both cases the pass band has been degraded by voltage division by the filter. Thus, for power supply filters it is best to use L-C-L tee configurations since these better achieve the proper mismatch conditions, but overall reductions in low frequency impedances are also required.

Thus we are led again to the important point that (mis)matching conditions finally determine most of the effectiveness of feedthrough filters. As is well known for lumped circuit filters, the sharpness of the insertion loss turn-on is improved by adding more stages to the filter. This is illustrated in Fig. 23 which is for a five-segment transmission line filter with a C-L-C-L-C configuration otherwise similar to the three segment standard case (cf. Fig. 12).

If one is feeding unknown loads, an approximate impedance match of the final segment to the load as illustrated by Fig. 21 may arise inadvertently. This can be mitigated by using a greater number of filter segments. Thus, Fig. 24 shows a five-element sequence as in Fig. 23, but with $R_l = R_s = 0.1$ ohms; the multisection filter has been buffered against the adverse effects of the very small terminations (cf Fig. 21) even though it has capacitative end segments. One must still deal with the losses in the pass band, however.

Phase Shift Considerations - The discussion up to now has concentrated on the insertion loss properties of the filters. One must also be concerned with the large frequency dependent phase shifts which are induced by the feedthrough filters in the victim signals within their pass bands. If one must transmit signals with significant frequency spreads through the filter, the phase shift dispersion must be considered. Simple modification to the four-

pole analysis given earlier allows these phase shifts to be calculated easily. Detailed discussions of individual cases would unduly enlarge the scope of this report. As an example, however, the phase shifts corresponding to Figs. 12 and 14 are identical below 7 MHz, at which point they have reached 180°. The 90° point is at about 5 MHz; dispersion persists to the lowest frequencies, where phase shifts change linearly with frequency. Such results are typical, although, as with attenuation, loading conditions can greatly modify their magnitudes.

V. CONCLUSIONS AND SUGGESTIONS FOR FEEDTHROUGH FILTER IMPROVEMENTS

In this chapter we point out a number of conclusions about the behavior of feedthrough filter pins which are based on the analysis of the last chapter and additional information given here. We also compare the design and the calculated insertion loss for the simple coaxial feedthrough filter connector used in that analysis with those of a typical commercial filter pin. This allows us to suggest possible ways to improve on such filters.

As noted earlier, the criteria for an improved feedthrough filter connector are increased insertion loss in the stopband, or a more rapid increase in insertion loss with increasing frequency beyond the passband of the filter, or achievement of comparable insertion loss at lower cost. In all cases the standard of comparison is commercial feedthrough filter connectors.

We can summarize the conclusions of the foregoing analysis as follows:

Impedance Mismatch - The paramount factor for the achievement of large insertion loss in the stopband of an EMI feedthrough filter connector is production of large impedance mismatches between the adjacent filter sections and between the rf source and load and the filter sections adjacent to them.

Material Properties - Proper use of high permittivity barium titanate type materials in the capacitive elements and high permeability ferrite materials in the inductive elements allow such impedance mismatches to be achieved within the stringent size constraints of a feedthrough filter pin. The rf losses associated with both the dielectric and the magnetic elements are important in greatly reducing the effect of dimensional resonances and their attendant punch-throughs on filter performance. In general, the materials used for filter pin construction successfully eliminate these resonance punch-throughs. We wish to emphasize that the areas both of high permittivity dielectrics and of high initial permeability ferrites are mature materials research fields. As a result, one does not expect any significant improvement in the material properties required by EMI feedthrough filters. This is especially true for the ferrites where increased permeability above 100 MHz is highly desirable but unlikely to be achieved.

Saturation Problems - Because the ferrites used in EMI filter connectors begin to saturate magnetically in a field of a few Gauss, a connector carrying a current of a few amperes experiences a drop in the rf permeability and hence the impedance of the ferrite element. At currents in the 10-20 amp range this can cause a large decrease in the insertion loss in the stopband of a filter pin type connector.

In a multipin connector, the various pins are capacitatively coupled because of their close proximity. Hence if the insertion loss of a single pin is severely reduced, it can serve as a point of entry for rf on all the other circuits, thus effectively bypassing their own EMI filter pins. This is an example of the necessity of filtering all the leads which pierce the shielding box. The best method for eliminating this problem in severe cases is to bring the power lead in on its own physically separated filter connector designed to handle larger currents. This filter will necessarily be significantly larger than a simple filter pin. In less severe cases, magnetic saturation effects can be reduced by bringing the power lead in parallel through several physically separated filter pins in the multipin connector. These leads can be tied together just inside the shielding box to prevent load distribution problems.

Dr. H. M. Schlicke ("Artificial Ferrite, A Theoretical Feasibility Study," submitted to NRL, 31 Aug 1981) has suggested the use of powdered cores (fine iron particles in an insulating or semiconducting matrix) to reduce the magnetic saturation problem while still retaining significant rf permeability for EMI filter use. This interesting suggestion has not yet been thoroughly investigated.

At high rf signal levels dielectric saturation and even dielectric breakdown can occur in the high permittivity materials as can permittivity variations due to rf heating. This problem arises chiefly in filter circuits which use large capacitance (and hence thin) elements.

Source and Load Impedances - The source and load impedances play an important role in the behavior of the filter. In general, one cannot design or choose a filter without knowing what these impedances (or at least their range of values) are. Typically, signal processing circuits will have impedances of 50 ohms or greater while power carrying circuits have 0.1 ohm or less. Thus, if one uses three-element filters, C-L-C pi filters are best for signal circuits and L-C-L tee filters for power circuits. If the source or load impedance is complex, there exists the possibility of circuit resonances involving the filter which may require special design. These considerations emphasize that it is inadequate to specify the filter performance only at 50 ohms as is normally done by EMI feedthrough filter manufacturers. It is important that the effects of changing the termination impedances away from 50 ohms also be known to avoid unpleasant results.

Multi-element filters - Use of filters with more than three elements can be used to achieve two goals: (1) They have a sharper insertion loss rise at the edge of the stopband, (2) They are less sensitive to the source and load impedance variations.

Low Frequency Behavior - Much of the important filter behavior is determined by the low frequency insertion loss at the edge of the stopband. This is a region in which the filter elements can be approximated as lumped circuit elements. The above approximation is valid if the characteristic impedance of the dielectric elements is low and that of the ferrite elements is large compared to each other and to the filter terminations. For typical materials used in filter connectors, if the low frequency insertion loss is adequate, then the high frequency insertion loss (above 100 MHz) will also be adequate.

Phase shift effects - EMI filters inherently have a considerable variation in phase shift with frequency even for frequencies in the passband. Thus, in general, one cannot faithfully reproduce wideband signals passed through such filters.

Coaxial design - Comparison with commercial filter pin specifications - The primary purpose for choosing a coaxial filter pin design for the work discussed in this report is that it is simple and amenable to an exact analytical approach. This makes it possible to evaluate the effects of changing various filter parameters with confidence. This has led to many of the conclusions stated above.

It is important, however, to compare the calculated insertion loss vs. frequency curves for this coaxial design with the actual performance specifications of commercial filter pin connectors. Such a comparison is shown in Fig. 25. The NRL coaxial pi filter calculations shown are the same as those given in Fig. 13 and represent a pi filter with unequal capacitive elements to reduce the effects of the remaining dimensional resonances. A commercial filter with essentially the same stopband cut-on was chosen for comparison. The mechanical designs of the two filters appear as inserts in Fig. 25. The commercial filter chosen gives the sharpest available insertion loss increase with a stopband cut-on at approximately 10 MHz. The filter calculations performed here indicate that the simple coaxial design can achieve comparable or better insertion loss in the stopband as well as a sharper attenuation turn-on beyond the passband.

The relative simplicity of the coaxial design should reduce construction costs of these filters, an important factor in applications. In addition, with such a design it is easy to construct a five-element (C-L-C-L-C) double pin filter in the same space restrictions. The enhanced performance of such a filter including the still sharper increase in insertion loss beyond the pass-band is also shown in Fig. 25. As mentioned earlier, the attenuation characteristics of such multiple-element filters are inherently less sensitive to variations in the source and load impedances away from the standard 50 ohms. These considerations suggest that such coaxial filter pin designs should be constructed and tested to see if they actually achieve their calculated performance.

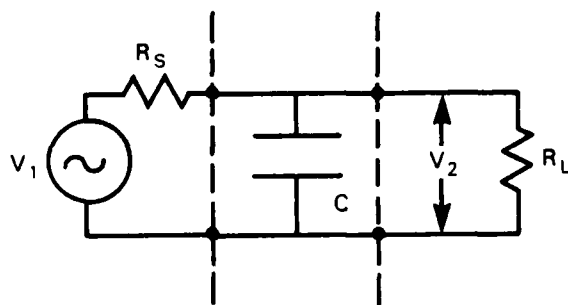


Fig. 1. Circuit with feedthrough capacitor inserted as filter element.

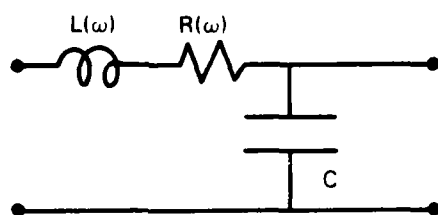


Fig. 2. Filter element modified by addition of ferrite bead.

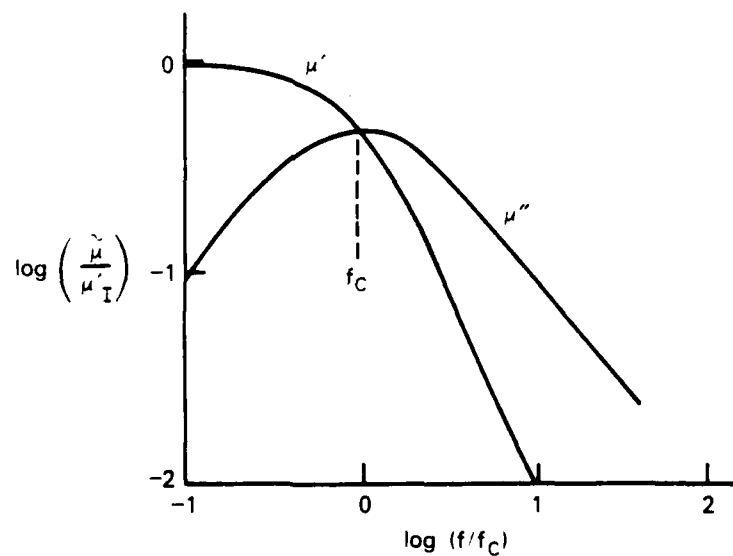


Fig. 3. Typical frequency dependence of ferrite initial permeability.

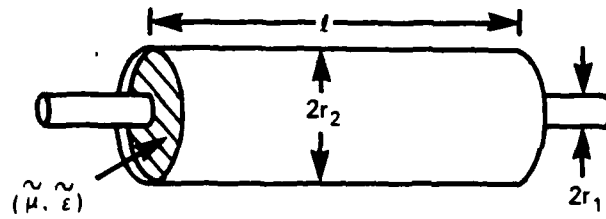


Fig. 4. Physical parameters of coaxial transmission line.



Fig. 5. Generalized four-pole network element.

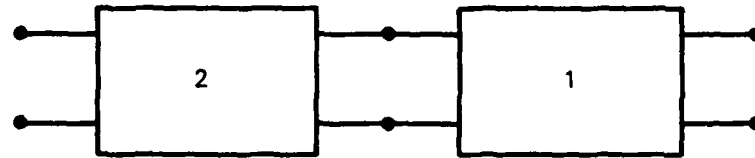


Fig. 6. Two four-pole elements in cascade.

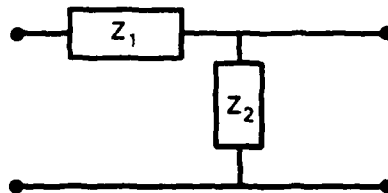


Fig. 7. Specific four-pole element discussed in text.

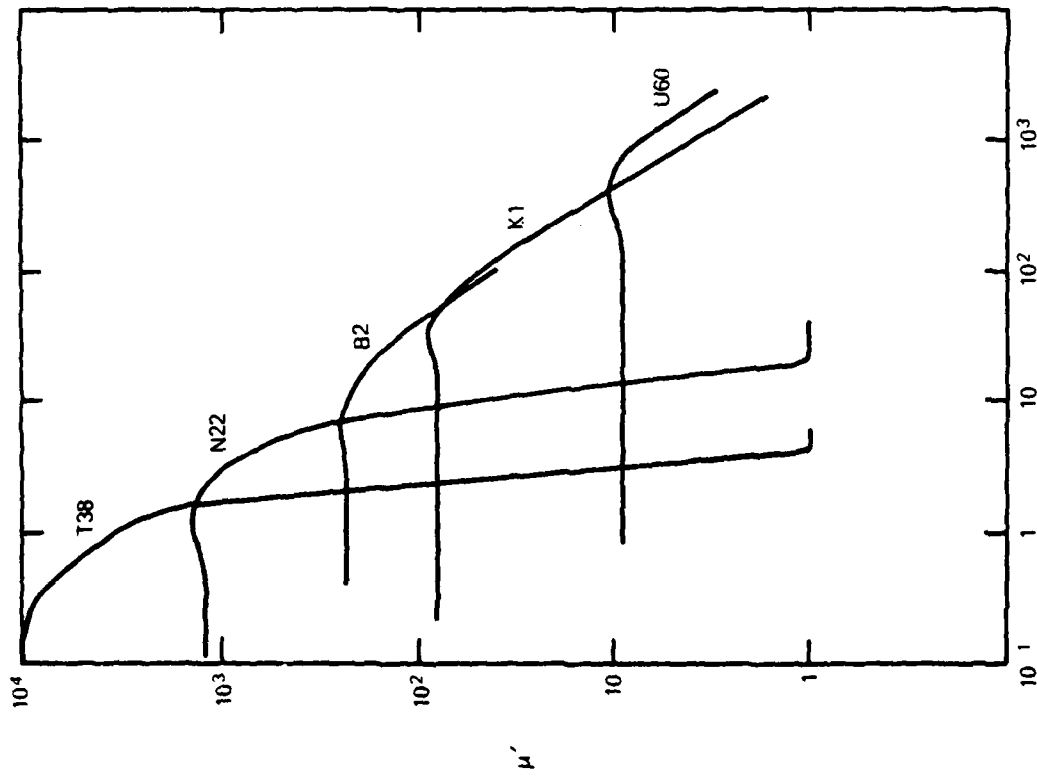


Fig. 8. μ' vs. f .

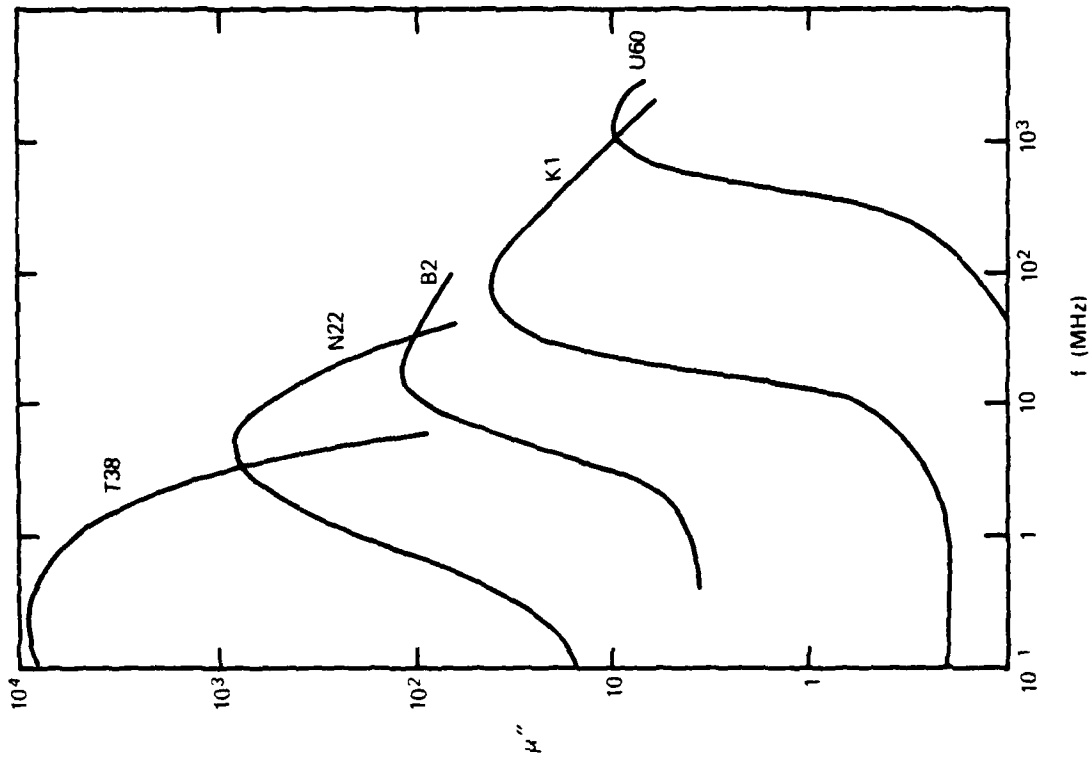


Fig. 9. μ'' vs. f .

Frequency dependence of initial permeabilities for representative ferrites.

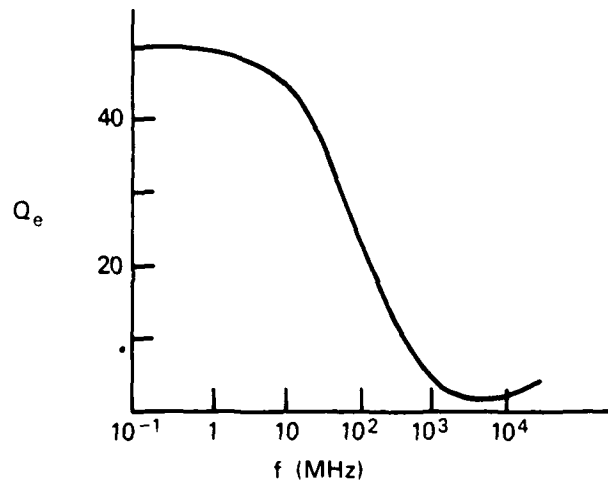


Fig. 10. Typical frequency dependence of quality factor $Q_e \equiv \epsilon' / \epsilon''$ for barium titanate dielectric material.

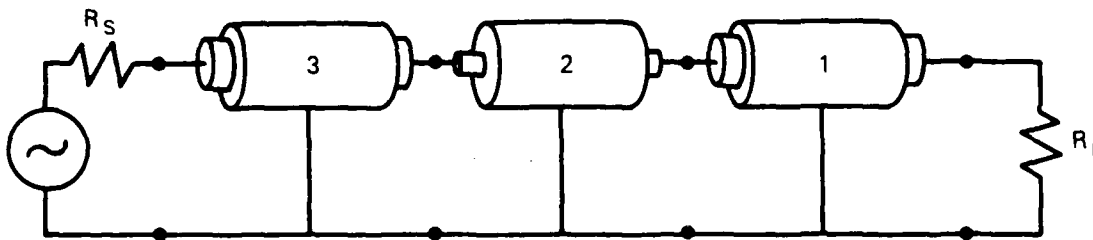


Fig. 11. Circuit as used for computation with feedthrough filter composed of three distinct coaxial segments.

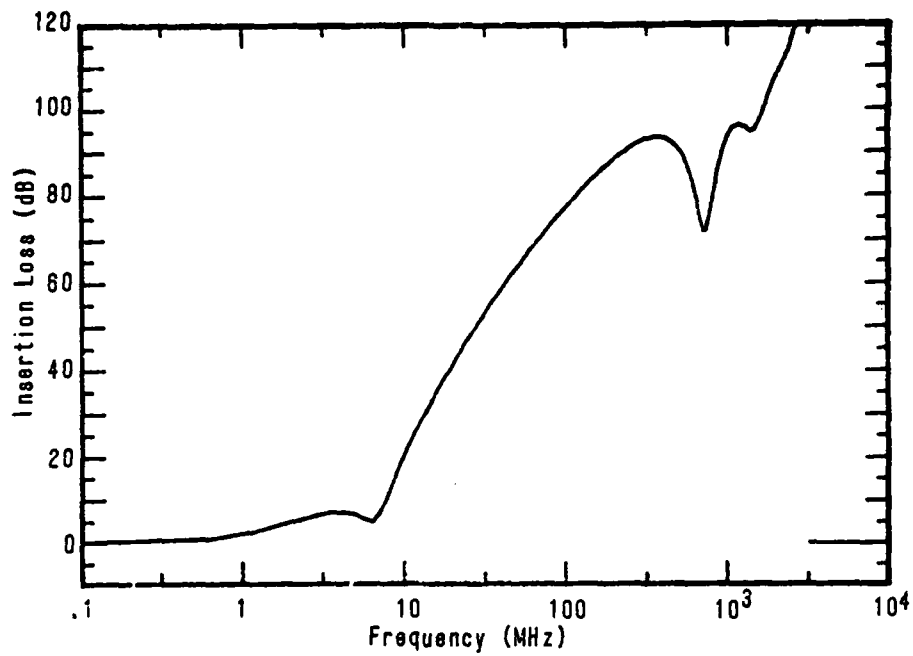


Fig. 12. Insertion loss vs. frequency for reference case filter. Conditions: $R_L = R_S = 50$ ohms, three segments each of length 0.5 cm. Segments 1 and 3 are $BaTiO_3$ filled and have $r_2/r_1 = 1.2$. Segment 2 is filled with B2 ferrite, $r_2/r_1 = 6$.

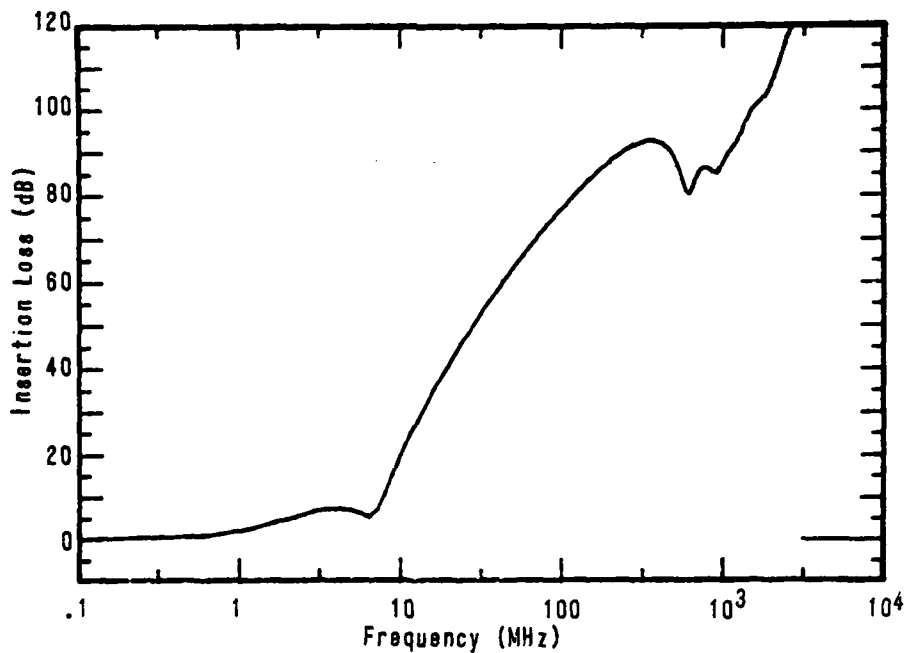


Fig. 13. Like Fig. 12, but segments 1 and 3 have lengths 0.4 and 0.6 cm.

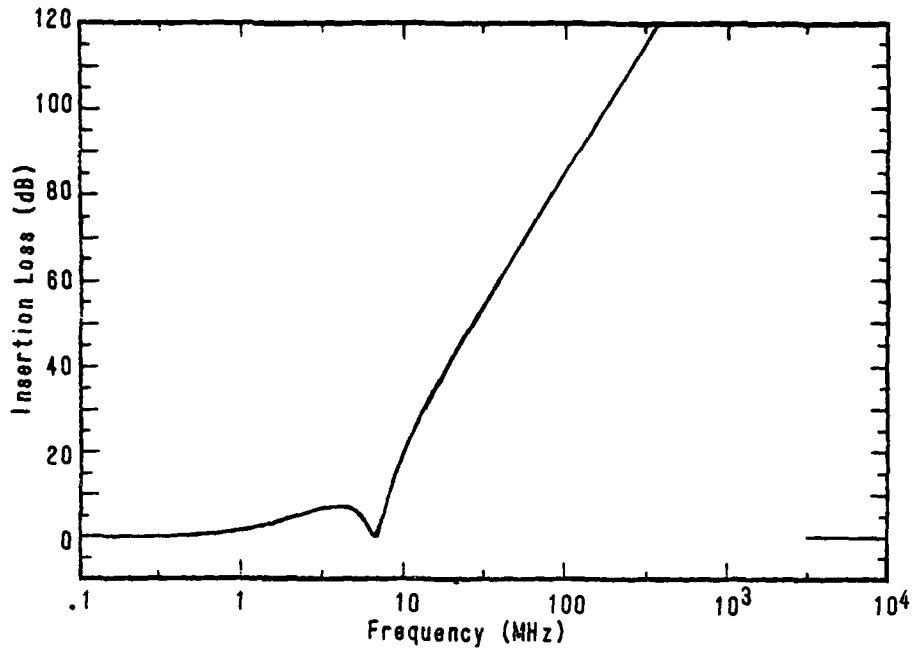


Fig. 14. Insertion loss vs. frequency for a lumped element CLC pi filter with $R_L = R_S = 50$ ohms; $C = 2600$ pF and $L = 0.43$ μ H to match low frequency characteristics of individual coaxial segments used for Fig. 12.

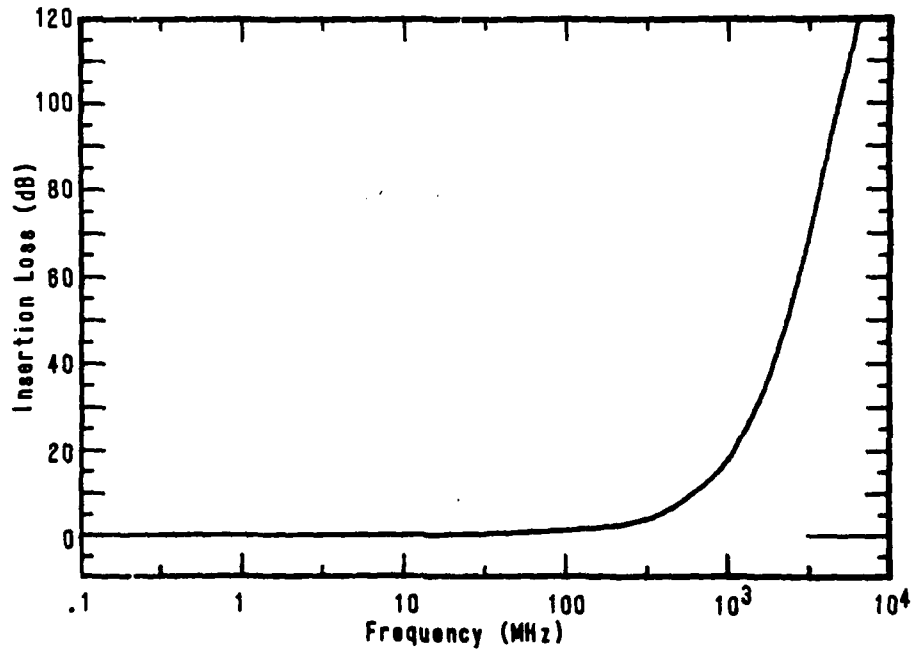


Fig. 15. Like Fig. 12 but $R_L = R_S = 2.61$ ohms; $r_2/r_1 = 6$ in segments 1 and 3, $r_2/r_1 = 1.009$ in segment 2. With these values all characteristic impedances match R_L , but propagation losses remain.

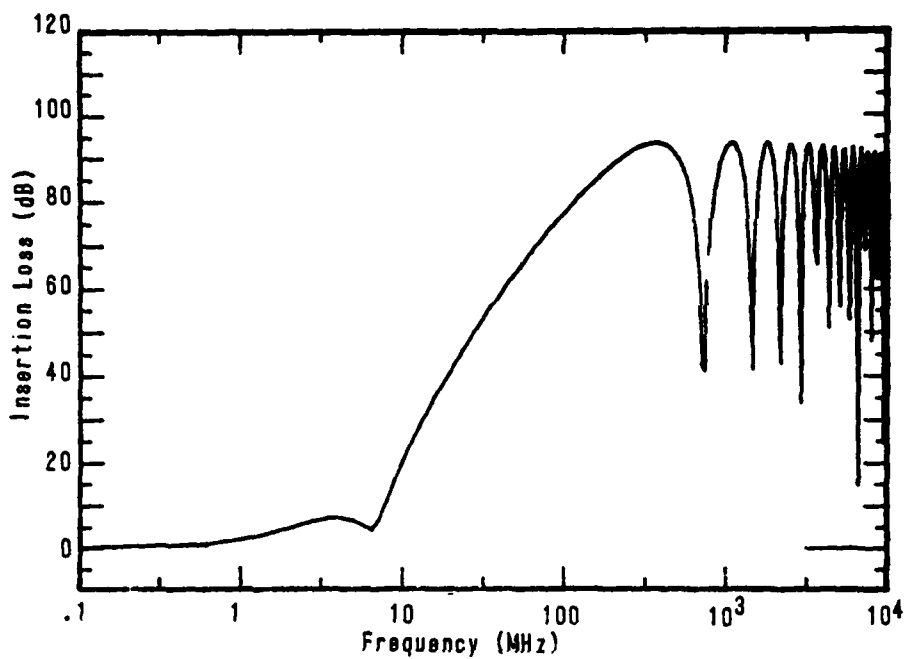


Fig. 16. Like Fig. 12 but losses in BaTiO₃ are eliminated. ϵ' fixed at 1700, ϵ'' at 0.

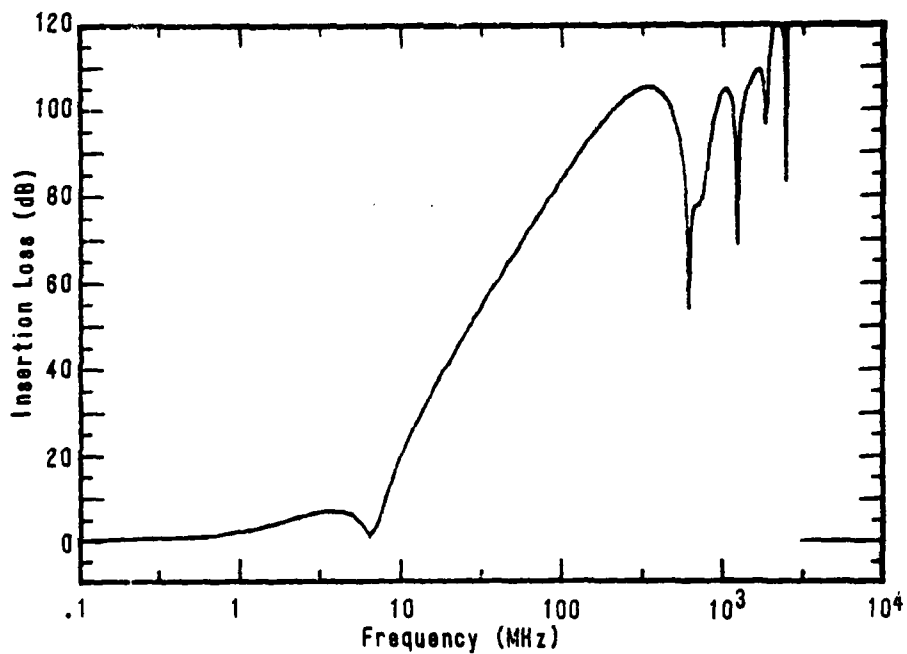


Fig. 17. Like Fig. 12 but dispersion in ferrite is removed. μ' fixed at 240, μ'' at 0.

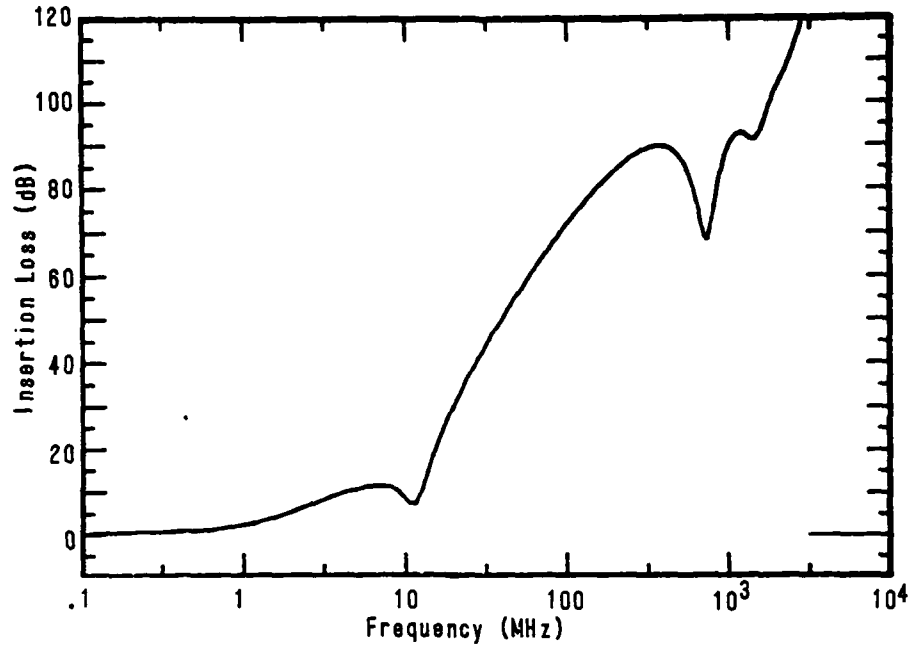


Fig. 18. Like Fig. 12 but with ferrite in segment 2 replaced by KI ferrite.

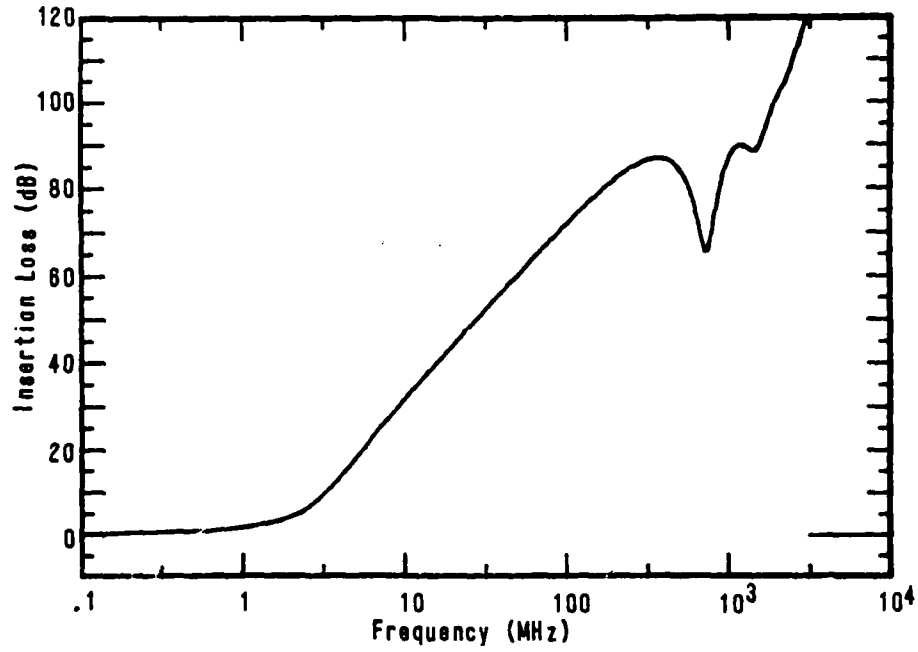


Fig. 19 Like Fig. 12 or Fig. 18 but with N22 ferrite substituted ($\epsilon' = 10$).

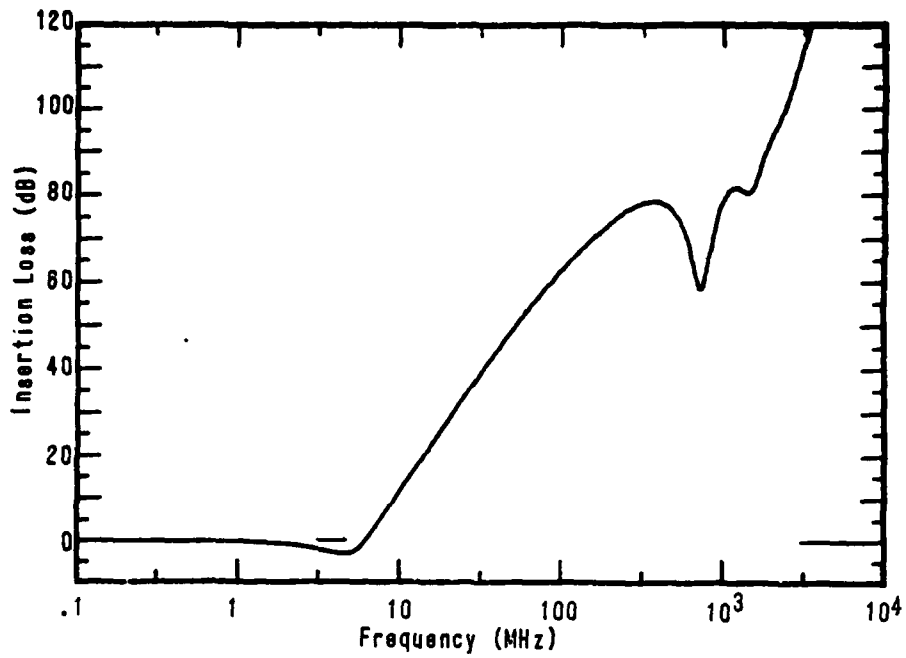


Fig. 20. Like Fig. 12 but with load R_L reduced to 5 ohms.

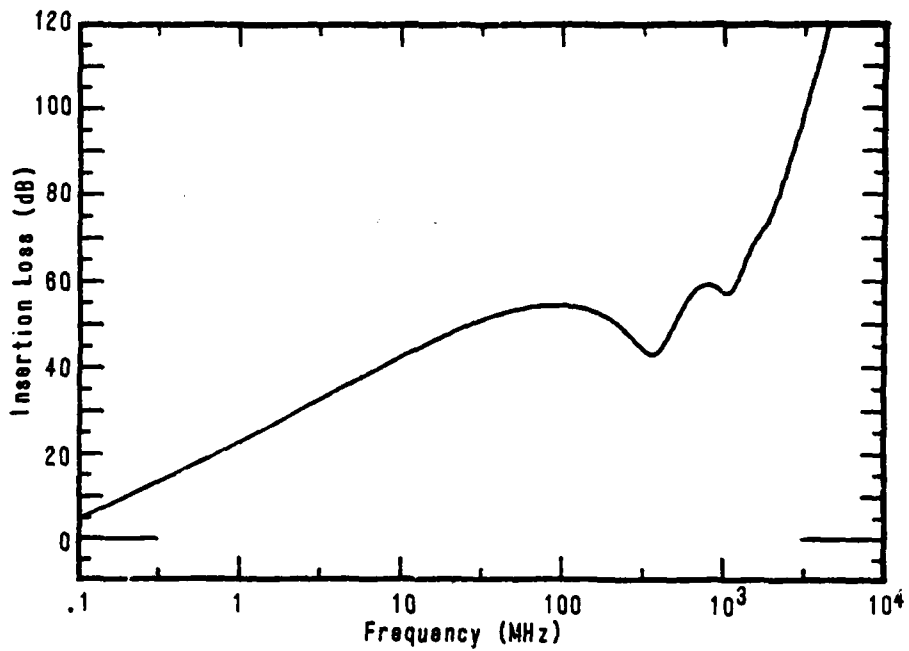


Fig. 21. Like Fig. 12 or Fig. 20, but with both R_L and R_S reduced to 0.1 ohm.

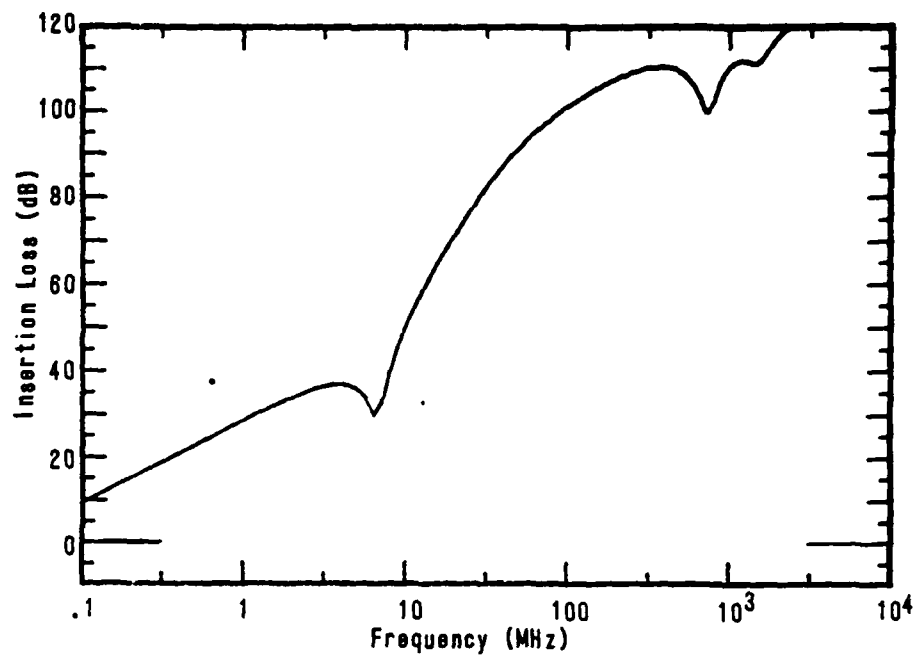


Fig. 22. Insertion loss vs. frequency for three segment L-C-L filter rather than C-L-C as in Fig. 21 with $R_L = R_S = 0.1$ ohm; L and C segments are the same in the two cases.

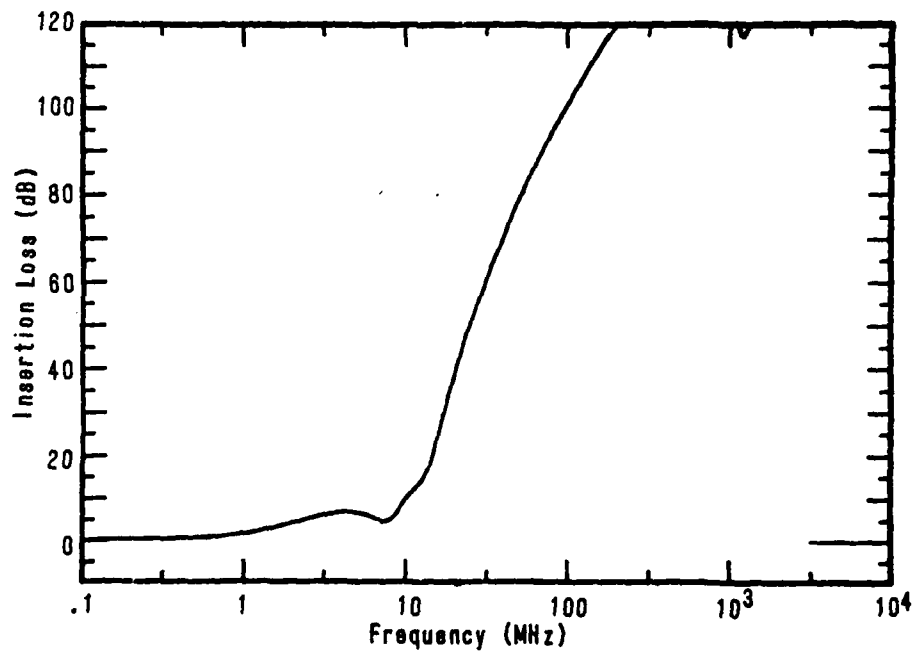


Fig. 23. Insertion loss vs. frequency for five segment filter composed like reference case Fig. 12, but with each segment length 0.3 cm; segments 2 and 4 ferrite loaded. $R_L = R_S = 50$ ohms.

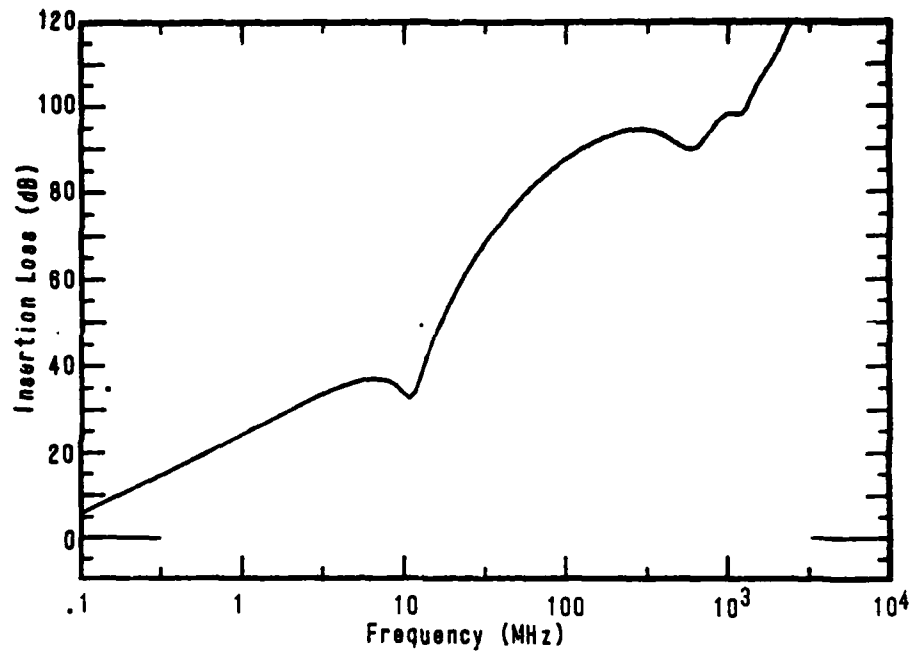


Fig. 24. Like Fig. 23 but with R_L and R_S both reduced to 0.1 ohm.

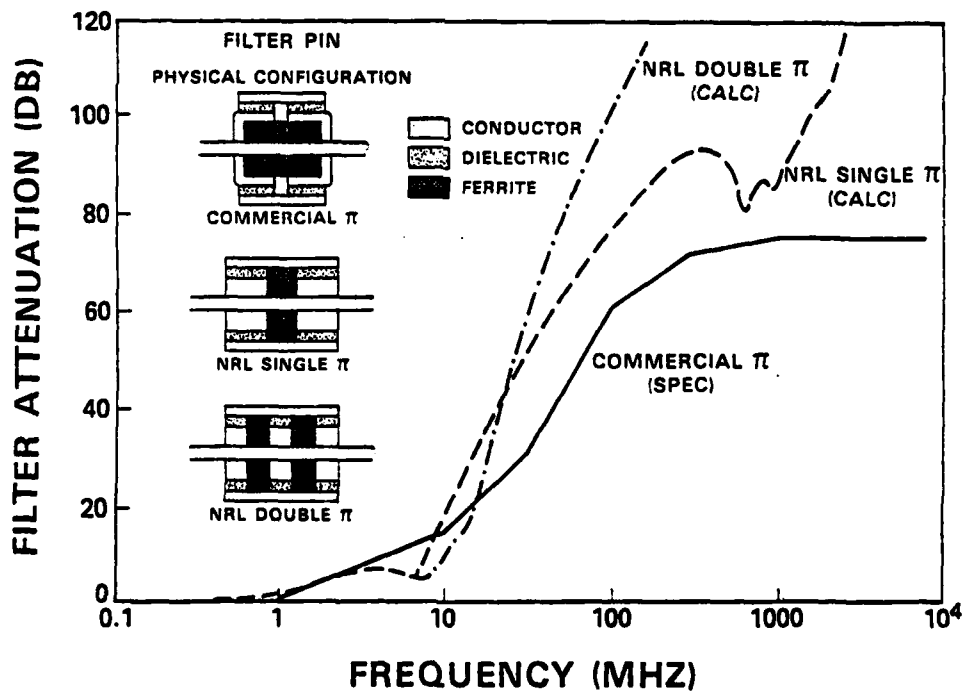


Fig. 25. Comparison of theoretical coaxial filter attenuations (cf. Figs. 13 and 23) with specifications for a commercial filter similarly loaded.